Available online at www.sciencedirect.com
ScienceDirect
Quaternary Research 67 (2007) 371–382
QUATERNARY RESEARCH
www.elsevier.com/locate/yqres

Control of wind strength and frequency in the Aral Sea basin during the late Holocene

Philippe Sorrel [a,*,1], Hedi Oberhänsli [a], Nikolaus Boroffka [a], Danis Nourgaliev [b], Peter Dulski [a], Ursula Röhl [c]

[a] *Sektion 3.3, GeoForschungsZentrum, Telegraphenberg, D-14473 Potsdam, Germany*
[b] *Faculty of Geology, Kazan State University, Kazan, Russia*
[c] *DFG Research Center for Ocean Margins (RCOM), Bremen University, Leobener Strasse, D-28359 Bremen, Germany*

Received 19 December 2005
Available online 1 February 2007

Abstract

Changing content of detrital input in laminated sediments traced by XRF scanning and microfacies analyses reflect prominent variations in sedimentation processes in the Aral Sea. A high-resolution record of titanium from a core retrieved in the northwestern Large Aral Sea allows a continuous reconstruction of wind strength and frequency in western Central Asia for the past 1500 yr. During AD 450–700, AD 1210–1265, AD 1350–1750 and AD 1800–1975, detrital inputs (bearing titanium) are high, documenting an enhanced early spring atmospheric circulation associated with an increase in intensity of the Siberian High pressure system over Central Asia. In contrast, lower titanium content during AD 1750–1800 and AD 1980–1985 reflects a diminished influence of the Siberian High during early spring with a reduced atmospheric circulation. A moderate circulation characterizes the time period AD 700–1150. Unprecedented weakened atmospheric circulation over western Central Asia are inferred during ca. AD 1180–1210 and AD 1265–1310 with a considerable decrease in dust storm frequency, sedimentation rates, lamination thickness and detrital inputs (screened at 40-μm resolution). Our results are concurrent with changes in the intensity of the Siberian High during the past 1400 yr as reported in the GISP2 Ice Core from Greenland.

Keywords: Chemical composition; Laminated sediments; Wind dynamics; Siberian High; Aral Sea; Late Holocene

Introduction

Despite a growing understanding of the regional impacts of global climate change during the last few thousand years (Bradley, 2000, 2003; Briffa, 2000; Crowley, 2000; Bond et al., 2001; Mann and Jones, 2003; Cook et al., 2004; Moberg et al., 2005), little attention has been granted to the Aral Sea basin. Since western Central Asia is situated at a confluence where different climate dynamics control the hydrology and environmental conditions (Small et al., 2001; Khan et al., 2004; Sorrel et al., 2006), the Aral Sea is an important archive for studying possible feedbacks between relevant climate features and their driving forces. Today the moisture distribution is controlled by the North Atlantic Oscillation (NAO) when the system is in a negative phase (Aizen et al., 2001), whereas draughts are possibly controlled by ENSO as proposed by Barlow et al. (2002), Khan et al. (2004) and Nezlin et al. (2005). Precipitation, which essentially occurs during winter and early spring in the deserts of Central Asia (Lioubimtseva et al., 2005; Nezlin et al., 2005), is associated with moisture originating from the eastern Mediterranean and migrates along a northeast trajectory to western Central Asia (Roberts and Wright, 1993; Aizen et al., 2001; Lioubimtseva, 2002; Sorrel et al., 2007).

In late spring and summer, precipitation is significantly reduced and heating of the desert lowlands in the Aral Sea basin causes local to regional advection responsible for numerous violent cyclones (>100 dust storms per year; Seredkina, 1960),

* Corresponding author. Fax: +33 231 565 757.
E-mail address: philippe.sorrel@unicaen.fr (P. Sorrel).
[1] Present address: Laboratoire Morphodynamique continentale et côtière (M2C), (UMR 6143 CNRS), Université de Caen Basse-Normandie, 24 rue des Tilleuls, F-14000 Caen, France.

0033-5894/$ - see front matter © 2007 University of Washington. All rights reserved.
doi:10.1016/j.yqres.2006.12.003

especially in areas adjacent to the northern shore of the Aral Sea (Zavialov, 2005). The dust storms are particularly favoured by northeastern, northern and northwestern winds (Romanov, 1961; Fig. 1) and represent the dominant mode of transport of detrital particles (Létolle and Mainguet, 1993; Orlovsky et al., 2005). Studies on dust storms in Central Asia have been mostly undertaken since the 1960s (Seredkina, 1960; Romanov, 1961; Middleton, 1986; Romanov, 1986; Zolotokrylin, 1996). Recently, Orlovsky and Orlovsky (2002) provided general characteristics on frequency, distribution and seasonality of dust storms in Central Asia, with a specific attention to the dust storms originating around the Aral Sea. Analyses of longer-term changes in zonal and meridional atmospheric circulation patterns in middle Asia have been documented by Subbotina (1995). However, most of these pioneering studies were limited to short periods of observations based on instrumental data from various sources, so that dust storm distribution and investigations on climate forcing mechanisms in the past are still insufficiently explored.

The principal obstacle for investigating late Holocene climate archives in western Central Asia is the lack of well-dated, high resolution sedimentary archives. Clastic material of lake sediments forming in arid and semi-arid environments reliably records changes of past atmospheric dynamics. In this study we present high resolution Ti and Ca XRF-scanning data, combined with microfacies observations of laminated sediments at Chernyshov Bay (Fig. 1), and extent knowledge of atmospheric circulation over western Central Asia in the past. The data reflect the variability of clastic input and shed light on changes in aeolian dynamics during the past 1500 yr in connection with the main pattern of spring atmospheric circulation in the Northern Hemisphere, the Siberian high pressure system.

Materials and methods

Coring locations and coring

In August 2002, two piston cores (Cores CH1 and CH2 with respective total lengths of 10.20 m and 6.20 m) were retrieved with a Usinger piston corer (http://www.uwitec.at) at Chernyshov Bay, in the northwestern Large Aral Sea (Fig. 1). These cores were collected 1 km off the shoreline (45°58.528′N, 59°14.459′E) at a water depth of 22 m. Core CH1 consists of sections 21, 22, 23, 27 and 28, whereas Core CH2 consists of sections 30, 31 and 32. The coring sites CH1 and CH2 were separated by a few meters. Correlations between Cores CH1 and CH2 were performed by matching laminations using photographs, bulk sediment density, magnetic susceptibility data and XRF scanning data (Sorrel, 2006).

Thin sections

For microfacies analyses and micro-XRF scanning, we prepared a continuous series of 10-cm-long sediment samples from the interval 4.28–4.98 m in Core CH2, corresponding to the interval 4.58–5.28 m in Core CH1 (i.e., Lithozone II plus 0.31 m in Lithozone I and 0.13 m in Lithozone III). The samples were freeze-dried and soaked with a transparent epoxy resin (Araldite® 2020; Vantico, Basel, Switzerland) and subsequently polished. An overlap of 4 cm between each thin section provided a detailed correlation at a scale of single laminations confirming the macroscopic correlation. Overall, 13 thin sections were analysed under parallel and polarized light with a microscope (Carl Zeiss Axiophot; Carl Zeiss, Germany). Magnifications used were 25× (overview) and 100× (measurement of lamination thickness and microfacies description). Thin

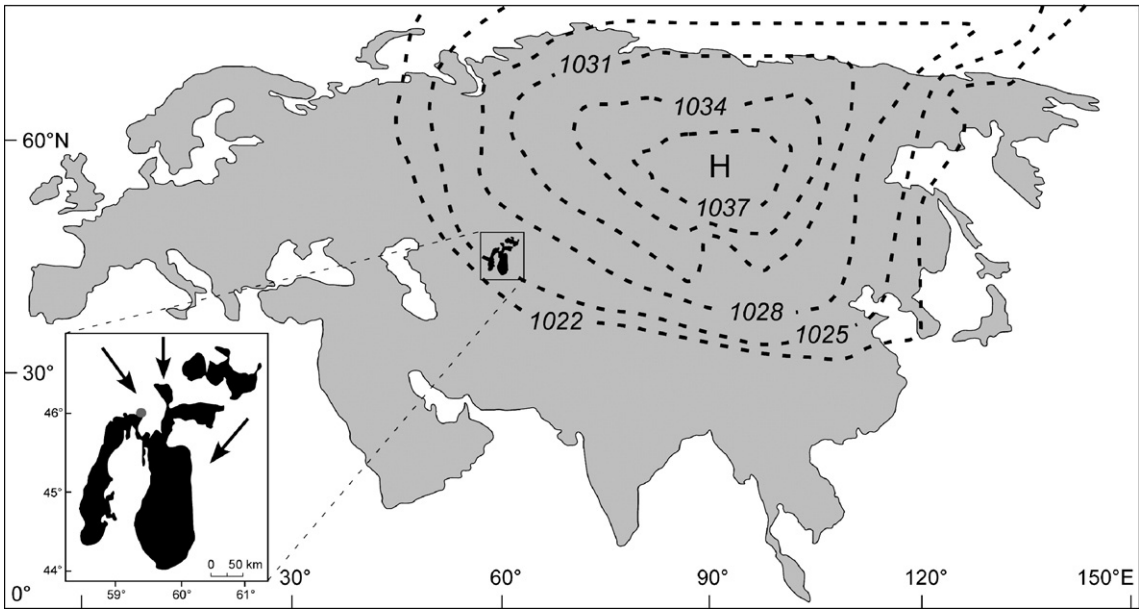

Figure 1. Location map of the study area and close-up on the Aral Sea (Chernyshov Bay: grey circle) with the dominant wind directions during the winter-early spring season (black arrows). Winter sea-level pressure (SLP) averaged over 1900–2001 (modified after Panagiotopoulos et al., 2005), showing the spatial extent of the Siberian High over Central Asia. Isobars are spaced every 3 hPa (dashed lines). H: High-pressure cell.

https://doi.org/10.1016/j.yqres.2006.12.003 Published online by Cambridge University Press

sections photographs were performed using a digital camera (Carl Zeiss Axiocam) and the software Carl Zeiss Axiovision 2·0. From thin sections, we semi-quantitatively determined changes in grain size, thickness of lamination, abundance of selected diatom species, and we searched for possible micro-disturbances in sedimentation.

X-ray fluorescence (XRF) scanning, magnetic susceptibility measurements and X-ray diffraction (XRD)

Titanium and calcium contents of the whole core were measured at Bremen University with a profiling X-ray fluorescence (XRF) core scanner (Jansen et al., 1998; Röhl and Abrams, 2000) at scanning steps of 1 cm using standard parameters (20 kV, 0.087 mA, 30 s detector accumulation time). When necessary, the measuring strategy was adjusted to avoid gaps. At GFZ Potsdam we measured the interval 4.58–5.28 m for elements Al, Ca and Ti at a 40-µm resolution. The profiling was performed with a micro X-ray fluorescence scanner (EAGLE III XL; Röntgenanalytik Meßtechnik GmbH) at 40 kV, 0.25 mA, 10 s detector accumulation time. For the scans we used the Araldite®-impregnated polished slabs, prepared for thin sections. Scans of pure Araldite resin (without sediment) indicated zero counts for investigated elements, thus proving that the resin does not bias the results.

Magnetic susceptibility was measured directly after core opening on the surface of split core halves with a Bartington MS2E sensor (GFZ Potsdam) at a resolution of 1 to 2 mm. For salt mineral identification we performed XRD analyses on selected samples from Core CH1 using a Siemens D 5005 diffractometer at the University Potsdam and used the program MacDiff 4·2·5 (Petschick, 2000) for mineral identification.

Lithology

Sediments retrieved from Chernyshov Bay (Fig. 2) consist of greenish to greyish silty clays and dark water-saturated organic mud with sporadically intercalated more sandy material. The sediments, which are finely laminated, comprise material of variable origin (terrigenous, biogenic and chemogenic) and size (from clay and fine silt to fine sand with mollusc shell fragments). Chemical precipitates, such as gypsum, occur as dispersed microcrystals in the sediment (G_2, G_3) and discrete layers (G_1) (Fig. 2). Neither erosive discontinuities nor features of bottom traction are observed in the core. The laminated character of Core CH1 indicates probable settling of various autochthonous and allochthonous particles from the water column during seasonally varying hydrographic conditions.

Three lithological units are recognized:

- Between 0.00 and 4.88 m (Lithozone I), the sediment is mostly composed of a grey silty to sandy clay intercalated with organic mud horizons, whereas the uppermost part (0.00–0.50 m) consists entirely of a dark, organic, finely laminated mud.
- Lithozone II (4.89–5.15 m) is characterized by a horizon of laminated gypsum at its base (G_1: 1 cm thick) overlain by a 1-cm-thick horizon consisting of brownish thinly laminated sediments. The latter horizon is overlain by a 12.5-cm-thick interval of yellowish thinly laminated sediments which in turn are progressively replaced by brownish thinly laminated sediments (11.5-cm-thick interval).
- Between 5.15 and 10.20 m depth (Lithozone III), the sediments consist of a dark silty to sandy organic mud, often water-saturated and very rich in organic matter including allochthonous aquatic plant remains. The plant remains occur both as a dispersed phase in the matrix and as partly decayed fragments that constitute organic horizons. These sediments are characteristic of dysoxic to anoxic bottom-water conditions.

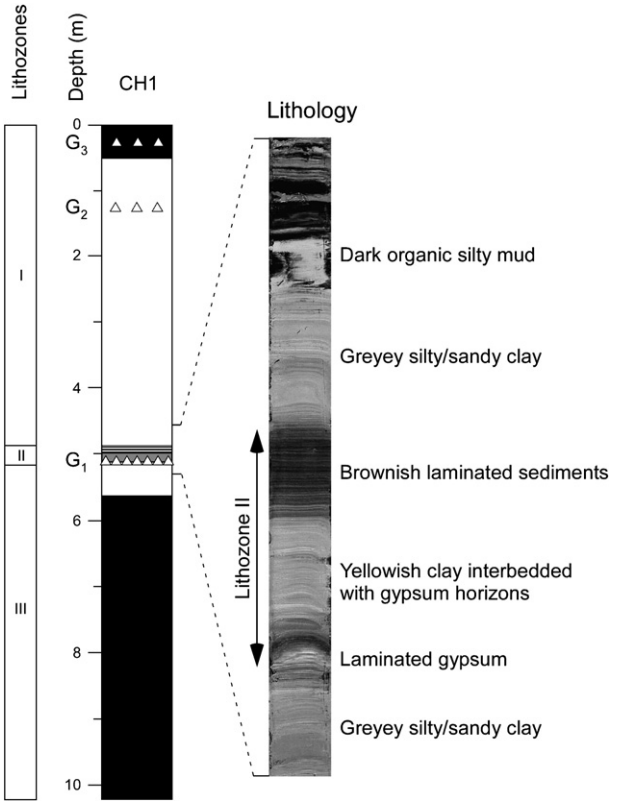

Figure 2. Simplified stratigraphic log of Core CH1 (10.20 m) with lithology of Lithozone II. Lithozones I–III and gypsum horizons G_1–G_3 are described in the text.

No turbiditic sediments have been recognized. The hydro-chemical conditions at Chernyshov Bay today are very pronounced. In 2002, a strong pycnocline had developed that maintains and stabilises an underlying anoxic deep-water body (Friedrich and Oberhänsli, 2004), which in turn influences the sedimentation and prevents from bioturbation. Hence, sediments from Chernyshov Bay show mostly well-preserved laminations.

Chronology

In Core CH1, AMS radiocarbon ages (Table 1) were determined using the filamentous green alga *Vaucheria* sp.

https://doi.org/10.1016/j.yqres.2006.12.003 Published online by Cambridge University Press

Table 1
Radiocarbon dates for section CH1

Sample name	Core depth (m)	Lab no.	^{14}C yr BP	Cal yr BP	2 SD	Dated material
Nourgaliev et al. (2003)[1]	1.50	KSU 2	435	480	120	*Vaucheria* sp.
Nourgaliev et al. (2003)[2]	4.80	KSU 3	640	655	65	*Vaucheria* sp.
Aral 27 209–212 cm	6.55	Poz-12279	1160	1062	110	*Vaucheria* sp.
Aral 27 269–271 cm	7.15	Poz-4762	1395	1300	30	*Vaucheria* sp.
Aral 28 40–45; 52–54 cm	7.95	Poz-9662	1480	1355	30	molluscan shells
Aral 28 112–114 cm	8.50	Poz-4760	1515	1395	25	*Vaucheria* sp.

AMS ^{14}C ages from this study were measured at Poznañ Radiocarbon Laboratory (Poland). Radiocarbon ages were corrected to calibrated (cal) ages using the IntCal04 calibration curve (Reimer et al., 2004). They indicate values with 2 standard deviations (95% of confidence).

and $CaCO_3$ from mollusc shells, which were successively picked from the washed sediment sample and carefully cleaned from adhering particles. Algae were then stored in distilled water within a glass vessel. For each sample, AMS ^{14}C dating was performed using between 0.2 and 1.0 mg of pure extracted carbon. An age model for Core CH1 based on AMS radiocarbon dating is proposed in Figure 3.

Reliable dating for the upper 5 m of Core CH1 was obtained by correlation with the magnetic susceptibility record from parallel cores 7, 8 and 9 retrieved ca. 50 m apart from the studied cores (Nourgaliev et al., 2003; Sorrel, 2006). AMS ^{14}C dating on cores 7, 8 and 9 was performed on *Vaucheria* sp. This correlation gives an age of 480±120 cal yr BP at 1.5 m depth for Core CH1. In addition, the time interval represented by Lithozone II is temporally constrained between 655±65 cal yr BP at 4.8 m depth and ca. 770 cal yr BP at 5.15 m for the laminated gypsum (Sorrel et al., 2006). These results imply high mean sedimentation rates during the deposition of Lithozone I (3 cm yr^{-1} between 1.5 and 4.8 m), but conversely very low sedimentation rates for Lithozone II (~0.2 cm yr^{-1}). Supplementary ^{14}C dating performed on *Vaucheria* sp. provides 1062±110 cal yr BP at 6.55 m, 1300±30 cal yr BP at 7.15 m and 1395±25 cal yr BP at 8.50 m, while ^{14}C dating from mollusc shells indicates 1355±30 cal yr BP at 7.95 m implying relatively high mean sedimentation rates for Unit 3 (~1.5 cm yr^{-1} between 7.19 and 10.20 m). Moreover, based on a peak in ^{137}Cs at 0.39 m core depth reflecting the climax of the bomb period (ca. AD 1963–1964) (Heim, 2005), the top of Core CH1 is post-1950. This is concurrent with ^{210}Pb values measured both in the topmost part of Core CH1 (Austin, unpublished data) and in the Gravity Core Aral IX overlapping the first 0.5 m of Core CH1 (Heim, 2005). Our chronology is in accordance

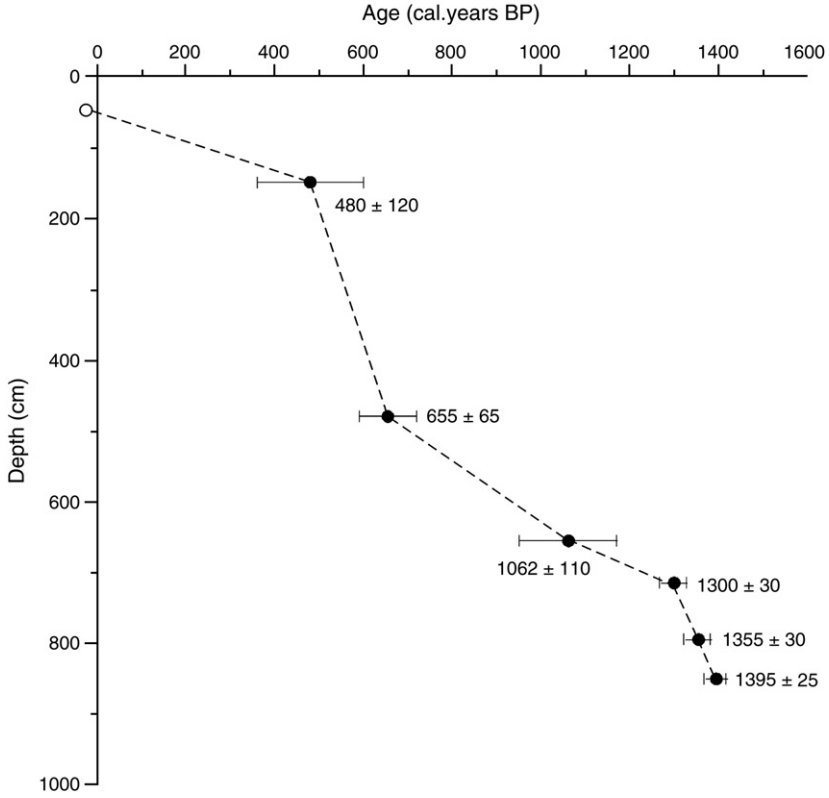

Figure 3. Age-depth relation for Core CH1 based on seven ^{14}C AMS dates. ^{14}C ages are calibrated and shown in calendar years.

https://doi.org/10.1016/j.yqres.2006.12.003 Published online by Cambridge University Press

with that of Austin et al. (2007), although a few divergences can be annotated downcore. These discrepancies are mostly due to the use of different calibration methods (Oxcal 3.10 in Austin et al., 2007; IntCal04 in this study) but the source of ^{14}C dating is the same (project CLIMAN). Due to a lack of dating of living algae samples from nearshore, no reservoir correction can be applied yet. This is work in progress.

Results

Physical and geochemical variability in Core CH1

Among seven elements analysed downcore using XRF scanning, only counts of calcium and titanium were selected, as their distribution can reliably highlight prominent changes in sediment composition and properties (Fig. 4). Other elements, like K and Fe, displayed either similar curves to Ti, or were mostly close to or below the nominal sensitivity of the instrument (average response for Mn: 119 cps, Sr: 69 cps). Calcium show the clearest signal, with highest values between 7.57–8.27 m, 5.14–5.15 m, 1.45–1.54 m and 0.00–0.25 m, where precipitates of gypsum are commonly found in the sediment (G_1–G_3; Fig. 2). Because higher values of calcium also match with phases of salinity increase as reflected by dinoflagellate cyst assemblages (Sorrel et al., 2006), we regard calcium as a proxy for changes in chemical water properties linked to reduced or enhanced evaporation in the surface waters. To show variability in the composition of detrital input at Chernyshov Bay, we chose titanium since it is clearly of terrigenous origin in the sediment fraction and influenced neither by productivity changes nor by early diagenetic processes. Relative abundance of Ti downcore further matches well with changes in the magnetic terrigenous input as reflected by the magnetic susceptibility curve. However, occasional mismatches between magnetic susceptibility measurements and relative abundance of Ti content do occur, probably related to selective dissolution of magnetic Fe oxides as they are redox sensitive (e.g., Demory et al., 2005). Nevertheless, both curves display similar features, namely high relative content in titanium corresponding to high magnetic susceptibility values. The lowest Ti and magnetic susceptibility values occur between 7.57–8.27 m, 5.14–5.15 m, 4.89–4.99 m and 0.00–0.25 m, corresponding in general to the gypsum-rich levels.

Close-up interval 4.58–5.28 m

In order to gain a better understanding of the sub-millimeter geochemical variability of individual laminae and to decipher the sedimentation process dynamics, we combined a microfacies analysis with XRF scanning for the interval 4.58–5.28 m at a very high resolution. The studied time period (ca. AD 1150–1400) corresponds to the lowermost part of Lithozone I, the

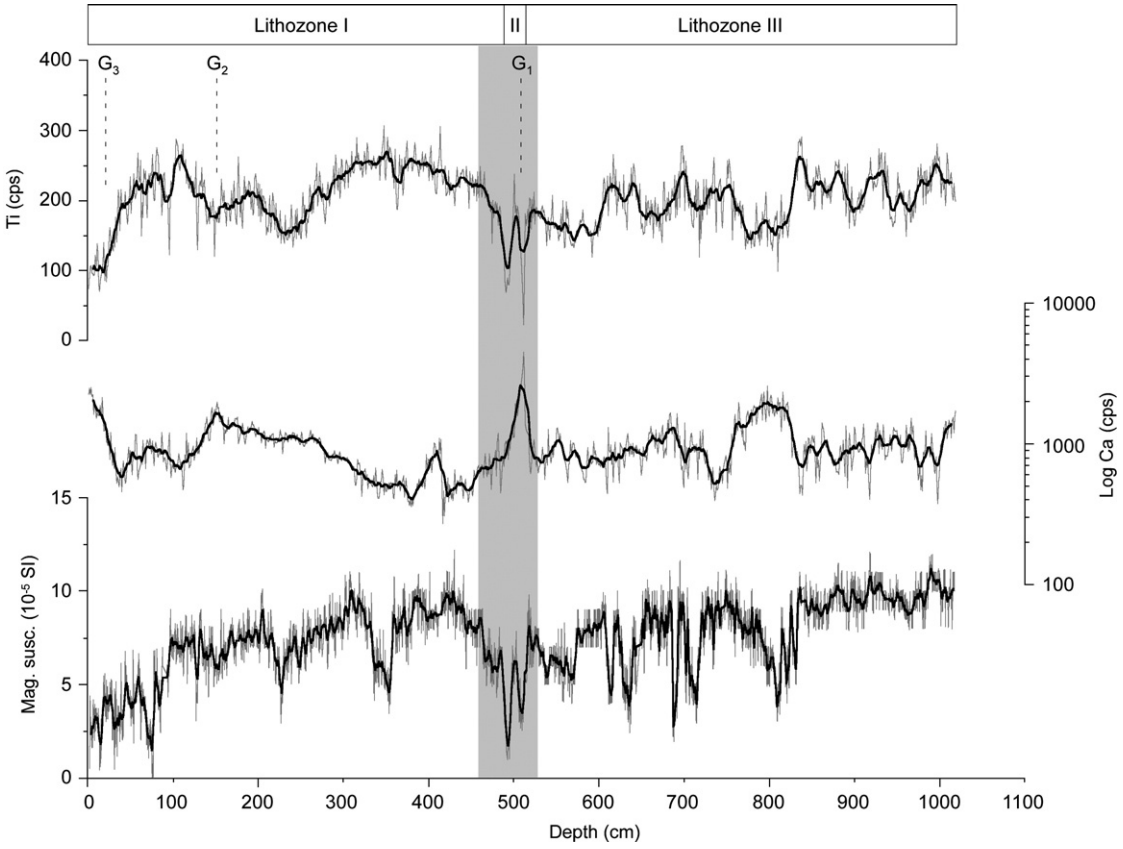

Figure 4. Stacked magnetic susceptibility (Mag. susc.) and X-ray fluorescence (XRF) data for calcium and titanium in Core CH1. Light grey thin lines represent original data; black thick lines are smoothed curves using a 21-point and 11-point running average for magnetic susceptibility and XRF data, respectively. The light-grey shaded areas refer to the close-up interval 4.58–5.28 m.

https://doi.org/10.1016/j.yqres.2006.12.003 Published online by Cambridge University Press

entire Lithozone II and the uppermost section of Lithozone III. In total, 1105 layers have been identified within this interval, 274 of them probably being of organic origin. The thickness of these layers ranges from ca. 0.025 to 20 mm. At the macroscopic scale, Lithozone II appears rather different to the adjacent Lithozones I and III, suggesting a major change in depositional processes. At the microscopic scale, these discrepancies are mostly related to changes in detrital inputs, implying changing dilution rates of biogenic material. Three distinct sedimentary microfacies (Fig. 5) are distinguished within the interval 4.58–5.28 m: (A) detrital-dominated sequence, (B) organic-dominated sequence, and (C) authigenic chemical precipitates.

Detrital-dominated sequences (4.58–4.89 m; 5.00–5.13 m; 5.15–5.28 m)

Detrital-dominated sequences consist of graded, non-graded and transitional discrete detrital layers without primary textural organization, which alternate with organic-bearing laminae. Detrital layers (Fig. 5.5) are composed of biogenic clasts (ostracods, diatoms, foraminiferans, molluscan shells) and detrital grains with grain sizes ranging from clay to medium [4–30 μm] and coarse [ca. 30–63 μm] silt particles. Isolated sand grains (up to ca. 170 μm) were observed in a few cases. Prevailing mineral phases are allochthonous carbonates from the surrounding Palaeogene marls (Bolle and Adatte, 2001),

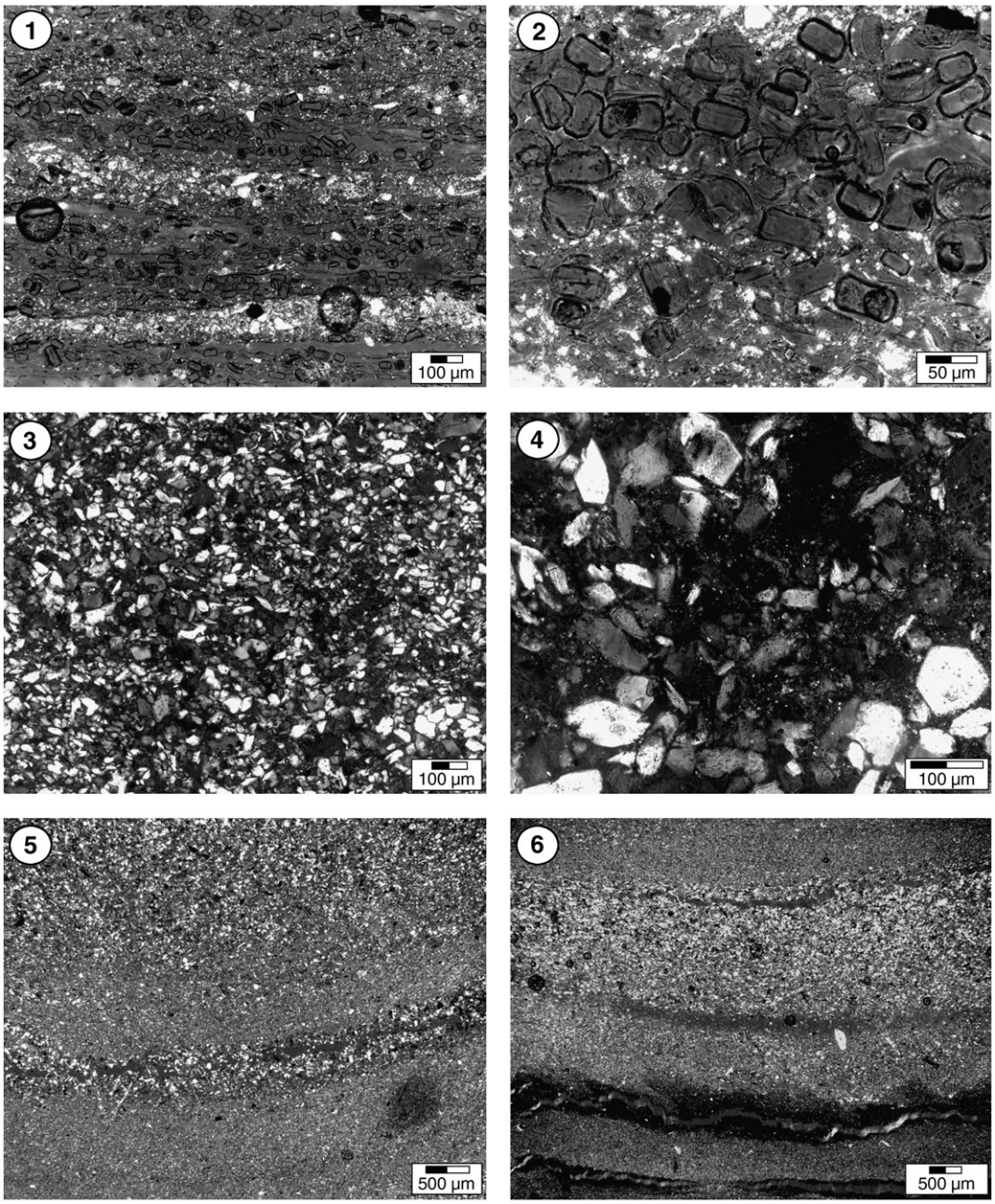

Figure 5. Thin-section images (crossed polarized light) of the three microfacies types identified: (1–2) organic-dominated ('varved-like') sequence (32W3; 4.89–5.00 m; microfacies 'B'); (3–4) authigenic chemical precipitates (32W5; 5.14–5.15 m; microfacies 'C'); (5–6) detrital-dominated sequence (32W18; 4.58–4.89 m; microfacies 'A').

https://doi.org/10.1016/j.yqres.2006.12.003 Published online by Cambridge University Press

sub-angular to angular xenomorphous quartz, feldspars, rounded glauconite grains, amorphous pyrite, gypsum crystals (5.15–5.18 m) and clay minerals. Detrital layers usually contain mixed-species diatom assemblages (*Actinocyclus* spp., *Cyclothella* spp., *Fragillaria* spp., *Navicula* spp., *Gyrosigma* spp., *Aulacoseira* spp., *Nitzschia* spp., *Amphora* spp., *Cocconeis* spp.); however, they are commonly dominated by the large centric diatom (>50 μm) *Actinocyclus* spp., which are often randomly distributed within the layer. Clay-sized barren laminae were observed in a few cases. The thickness of detrital layers varies from 0.025 to 20 mm, but most of them are >0.2 mm thick.

Organic-bearing laminae (see Fig. 5.6) occur more seldom. They are commonly matrix supported with a dominance of clay-sized detrital particles and medium silt-sized [ca. 4–25 μm] detrital particles. Organic-bearing laminae are characterized by higher contents in black organic matter and usually by higher abundance in diatoms, notably *Actinocyclus* spp. and *Navicula* spp. This would suggest a less detritally diluted and quieter deposition mode than during the deposition of the pure detrital layers.

Organic-dominated sequences (4.89–5.00 m; 5.13–5.14 m)

Organic-dominated sequences (Fig. 5.1) are characterized by a regular alternation of diatomaceous organic mud laminae and detrital laminae with no obvious primary textural organization. Detrital laminae are composed of detrital grains with grain sizes ranging from clay to angular medium [4–30 μm] and coarse [ca. 30–63 μm] silt particles. Isolated sand grains (up to ca. 100 μm) were observed in a few cases scattered in the detrital laminae. Prevailing mineral phases are allochthonous biogenic carbonates (mostly remains of coccoliths) with subordinate xenomorphous quartz, feldspars and clay minerals. The detrital laminae usually contain mixed diatom assemblages (most common species present are *Actinocyclus* spp. [4.88–4.97 m] and *Navicula* spp. [4.97–5.00 m], [5.11–5.12 m]); however, some are barren of diatoms (Fig. 5.1). The thickness of detrital laminae varies from 0.025 to 2.65 mm, but the majority of them are >0.1 mm (average thickness 0.3 mm). Diatomaceous organic mud laminae commonly consist of a mixture of organics and fine to medium [4–30 μm] detrital grains forming the matrix. These diatomaceous laminae also often occur matrix-free, consisting only of diatomaceous material. They are typically near-monospecific oozes of *Actinocyclus* spp. (Fig. 5.2). The thickness of diatomaceous mud laminae varies from 0.05 to 0.50 mm (average thickness 0.15 mm). Alternating couplets diatomaceous mud laminae-detrital laminae (although triplets are also occasionally observed based on the presence of an additional distinct detrital lamina) are probable seasonal deposits, assigned as "varve-like" sediments. XRD analyses conducted at 5.02 m and 5.07 m revealed the presence of halite in sediments (with characteristic intensity peaks at $2\theta = 31.718°$ and $2\theta = 45.487°$ in diffractograms), which matches well with highly saline conditions inferred by dinoflagellate cyst assemblages (Sorrel et al., 2006).

Authigenic chemical precipitates (5.14–5.15 m)

Authigenic chemical precipitates consist of isomorphic crystals of gypsum (20–60 μm) (Fig. 5.3–5.4). Authigenic deposits generally lack any matrix; however, they were occasionally observed slightly matrix-supported as well, with clay-sized detrital grains forming the matrix. Authigenic gypsum precipitates are usually barren of diatoms. The presence of gypsum crystals has been further confirmed by XRD analyses conducted on sediment samples at 5.15 m displaying typical peaks at $2\theta = 11.705°$, 20.802° and 29.193°.

Ultra high-resolution XRF scanning and microfacies analysis

As inferred from Figure 4, titanium is regarded as a reliable proxy for tracing changes in detrital terrigenous inputs at Chernyshov Bay. In the studied close-up interval (Fig. 6), the aluminum curve displays mirrored variations with Ti, suggesting that this element is similarly of terrigenous origin (mainly in the clay fraction), neither influenced by productivity changes nor by early diagenetic processes. In general, the thickness of the laminations follows the same trend as the Al and Ti distribution through the interval: the thicker the lamination, the higher Al and Ti count rates. This is especially obvious between ca. AD 1180 and 1360 (4.74–5.15 m) but less pronounced in the uppermost part of the interval (4.58–4.68 m). Conversely, the thinnest laminations correlating with the lowest Al and Ti values occur within the intervals 4.89–5.00 m and 5.13–5.14 m. To get a better understanding of the laminae composition, particularly the relation between biogenic and mineralogical grains, we include for each identified lamination the relative abundance of *Actinocyclus* spp. as well as a grain-size index corresponding to the averaged grain size measured on detrital particles (Fig. 6). In general, these curves are inversely correlated, especially between 4.58–4.68 m (microfacies A) and 4.74–5.15 m, where increased content in *Actinocyclus* spp. correlate with smaller grain size and vice versa. Moreover, plots of relative abundance of *Actinocyclus* spp. and lamination thickness also yield anti-correlated features throughout this interval, with lower content in *Actinocyclus* spp. corresponding to thicker laminations (4.58–4.68 m; 5.00–5.13 m; 5.15–5.28 m). The opposite pattern is evident in the upper part of Lithozone II (4.89–5.00 m; microfacies B).

Interpretation and discussion

Reconstruction of environmental dynamics from ca. AD 1150 to 1400

To infer the signals contained in the inorganic phases of the sediments, the pathway of the elements Al and Ti must be assessed. Ti, which is commonly concentrated in heavy minerals, is preferentially enriched in iron-titanium oxides concentrated in the clay and silt fractions. Because plots of Ti and Al show a very good correlation in the interval 4.58–5.28 m (Fig. 6), we propose that both elements are of similar origin (although Al is preferentially enriched in the clay fraction) and thus reflect changes in detrital input.

https://doi.org/10.1016/j.yqres.2006.12.003 Published online by Cambridge University Press

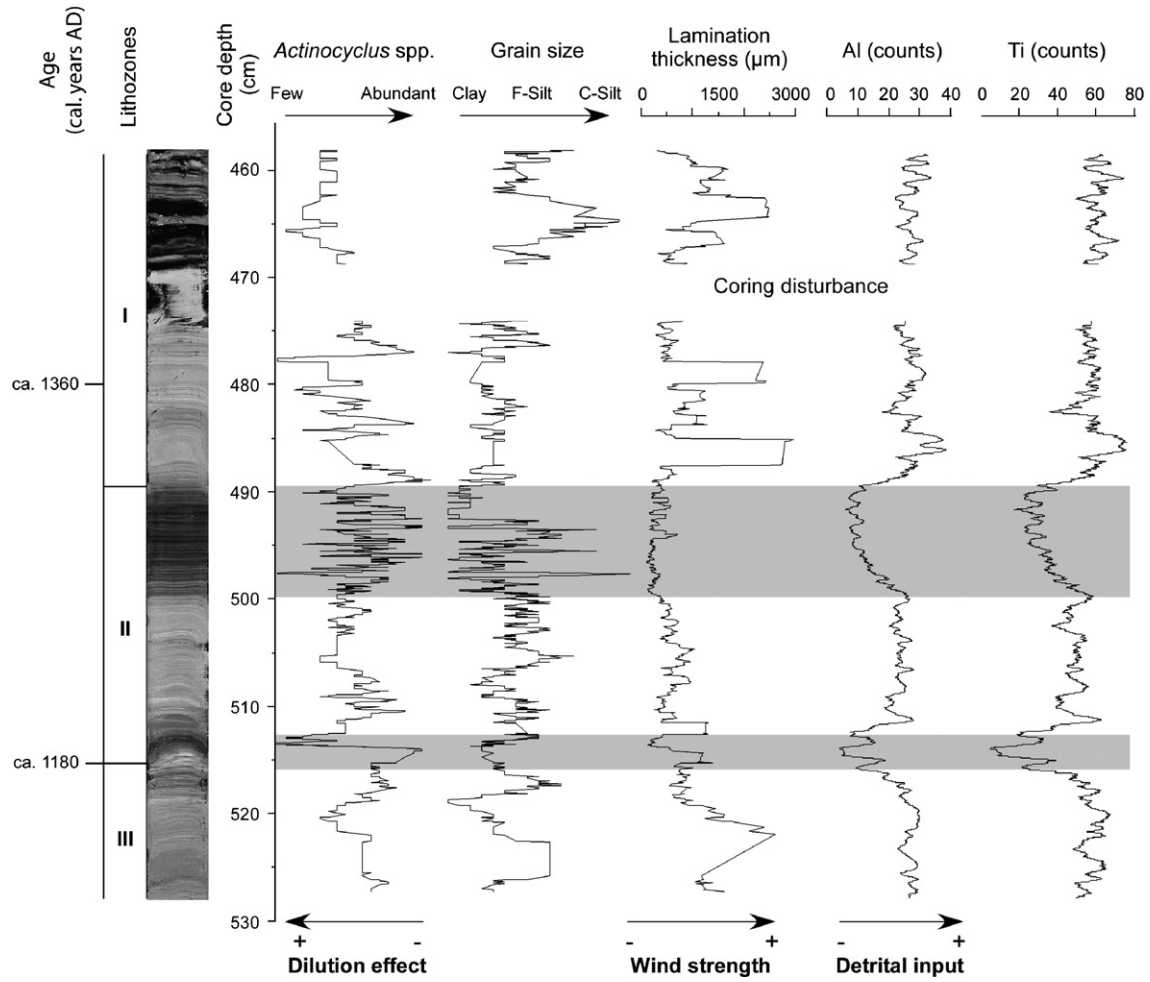

Figure 6. High-resolution XRF (Al, Ti: 40 µm) and microfacies (relative abundance of *Actinocyclus* spp., grain size and lamination thickness) palaeoclimatic proxy data for the close-up interval [4.58 m-5.28 m; ca. AD 1150–1400]. Plotted data are smoothed curves using a 9-point and 101-point running average for microfacies and XRF data, respectively. Shaded area corresponds to time periods characterized by a considerable decrease in dust storm frequency in the Aral Sea basin.

At Chernyshov Bay, the fluvial discharges from the Syr Darya and Amu Darya Rivers are remote from the coring location and are unlikely sources of detrital Ti-bearing particles to the coring site. Similarly, the riverine discharge from small ephemeral rivers eroding the adjacent hilly outcrops consisting of early and late Tertiary marls can hardly account for the high Ti content recorded in Core CH1. Hence we postulate that water-transported suspended particles are not important contributors to terrigenous particles at Chernyshov Bay.

A likely source of these detrital sediments, however, is evident. The Aral Sea lies in a basin characterized by semi-desert to desert conditions, and so aeolian remobilization of weathered sediment particles by dominant northeast winds is our proposed process of reworking, as reported earlier by Mainguet et al. (2002) and Singer et al. (2003). Extreme heating of the dark desert areas of Central Asia (Kyzyl Kum=black desert) indeed favours the formation of dust storms during the summer season (Orlovsky et al., 2005). During spring, regional pressure distribution in combination with rising temperatures over the continent cause the evaporation of the weak seasonal precipitation and the drying of the upper silty and sandy surface beds, both favourable conditions for the formation of dust storms (Orlovsky and Orlovsky, 2002). In the Aral Sea basin, a maximum frequency of dust events has been registered during early spring in the plain areas, including the Ustjurt Plateau and Central Karakum Deserts (>100 dust storms per year) and in the middle part of the Amu Darya River (Orlovsky et al., 2005). Hence, aeolian transport of particles is by far the dominant process for removal of detrital particles in the northwestern part of the Aral Sea which can realistically account for the high sedimentation rates recorded in Core CH1.

We therefore propose that variations in Al and Ti within Core CH1 are mainly the result of changes in the intensity of wind energy. Moreover, because both geochemical proxies and lamination thickness are positively correlated (i.e., a high content in detrital elements corresponds to thicker laminations suggesting a genetic relationship for these components), we hypothesize that the lamination thickness is also a reliable indicator of wind strength and frequency in the past.

As a whole, the most conspicuous changes in the frequencies of *Actinocyclus* spp. are anti-correlated with variations in lamination thickness (Fig. 6). They suggest that the abundance of *Actinocyclus* spp. in the sediment is linked to sedimentation processes rather than to productivity in surface waters,

https://doi.org/10.1016/j.yqres.2006.12.003 Published online by Cambridge University Press

reflecting the dilution of particles exposited on the lake bottom. As a result, with more (less) frequent dust storms, denser (weaker) detrital particle rain form on and through the water column, resulting in more (less) dilution of biogenic particles in laminations. A similar phenomenon can be observed from other diatom species (e.g., *Navicula* sp.), whose abundance in sediment inversely matches changes in lamination thickness (not shown here). This implies that some of the biogenic grains found at the coring location are not *in situ* but may originate from the remobilization of sub-contemporaneous nearshore sediments. Grain size can also serve as a further proxy for characterizing wind energy: the stronger the storms, the coarser the detrital grains brought into the system (Fig. 6).

Using geochemical and sedimentological proxies at high resolution, the following picture of wind dynamic evolution can be drawn for the interval 4.58–5.28 m, covering the time interval ca. AD 1150–1400. High content in Al and Ti, thick laminations and low abundance of *Actinocyclus* spp. suggest elevated aeolian detrital inputs at Chernyshov Bay in the uppermost part of Lithozone III (ca. AD 1150–1180), related to prominent dust storms in the Aral Sea region (microfacies A). The lithological transition II/III, however, is characterized by a drastic waning of wind strength and frequency. Minimal values of Ti and Al in the gypsum layer (microfacies C) at ca. AD 1180 document decreasing detrital inputs at that time associated to rarer and weaker dust storms, during a pronounced salinity increase in the Aral Sea (Sorrel et al., 2006). Subsequently, on the basis of higher values of detrital inputs (Ti, Al), thicker laminations containing coarser grains and enhanced dilution of *Actinocyclus* spp. in the sediments, stronger and more frequent dust storms are inferred in the lower part of Lithozone II (5.13–5.00 m; ca. AD 1210–1265). Wind dynamics rapidly weakened upwards (5.00–4.89 m; ca. AD 1265–1310) as reflected by drastically lower detrital inputs (Ti, Al), thin brownish "varve-like" sediments containing oozes with abundant *Actinocyclus* spp. (microfacies B) and low sedimentation rates (<0.2 cm yr^{-1}). Between ca. AD 1360 and 1400, prominent and frequent dust storms responsible for high sedimentation rates in Lithozone I (~ 0.8 cm yr^{-1}; microfacies A) are implied through elevated values of Al and Ti, frequent occurrences of thicker laminations and enhanced dilution of diatoms.

Control of wind strength and frequency in the Aral Sea basin

Wind dynamics regulating the occurrence of dust storms, and thus the detrital eolian input into the Aral Sea, are an important factor in the Central Asian climate system. Maximum frequency of dust storms and high wind speeds occur during the spring months (Létolle and Mainguet, 1993), favoured by an increase in intensity of the general circulation due to the seasonal warming, more energetic cyclone activity and cold-wave intrusions (Orlovsky et al., 2005). Therefore, because early spring wind dynamics are the result of atmospheric circulation on a broad scale associated with seasonal temperature and pressure gradients, it is crucial to examine connections of wind with other climate dynamics. Recent studies based on instrumental data (air temperature) and modelling, for instance, demonstrated a possible influence of the El Nino Southern Oscillation (ENSO) in western Central Asia (Gruza et al., 1999; Barlow et al., 2002; Khan et al., 2004).

In western Central Asia the seasonal wind field is controlled by the Siberian High (SH) and the Tibetan Plateau thermal forcing. The Siberian High anticyclonic feature is broadly recognized as the dominant mode of winter and spring climate over Eurasia (Sahsamanoglou et al., 1991; Savelieva et al., 1991; Panagiotopoulos et al., 2005). Its intensity and geographical position strongly control precipitation and atmospheric circulation patterns (meridional or zonal) at mid-latitudes of Asia (Aizen et al., 2001), although its influence on snow-cover extent is questionable (Clark et al., 1999). During early spring, the Aral Sea basin in western Central Asia is influenced by the western periphery of the SH and experiences air mass intrusions from the north, northeast and northwest (Orlovsky et al., 2005; Zavialov, 2005). A recent study by Meeker and Mayewski (2002), based on instrumental data, shows that maxima in non-seasalt potassium (nssK) deposition in Greenland correlate to a spring strengthening of the SH pressure system, which obviously has an impact on the wind pattern in western Central Asia. This proxy has been also used by Rohling et al. (2002) for examining the influence of winter and spring intensity of the SH on Aegean sea-surface temperatures. Therefore, in western Central Asia, time periods characterized by increased (reduced) content in detrital input (Ti) probably stem from stronger (weaker) and more westward (eastward) SH during enhanced (reduced) spring meridional (zonal; Clark et al., 1999) atmospheric circulation. The organization of the major long-wave pattern, when a meridional circulation mode prevails, results in increasing frequency of the synoptic processes with large-amplitude stationary waves and low pressure systems with small barometric gradients (Subbotina, 1995). It has to be kept in mind, however, that years with prolonged ice-cover extent in the Aral Sea basin (April-May) may considerably reduce the aeolian remobilization of sediment particles and occurrence of early spring dust storms, independently of the strength and position of the Siberian High (Clark et al., 1999).

On the other hand, the Tibetan Plateau thermal forcing, which leads to dry and hot conditions to the west, is crucial for the summer circulation in the Aral Sea basin (Duan and Wu, 2005). The development of lower-layer divergence and upper-layer convergence over the western side of the Tibetan Plateau, with prevailing E–NE winds at the surface, results in the formation of multiple dust storms during summer in the Aral Sea basin. However, since the maximum frequency of dust storms occur during the early spring months we rather focus here on the mechanism regulating changes in wind dynamics in W Central Asia, namely the Siberian High.

Meeker and Mayewski (2002) documented prominent variations in strength of the Siberian High for the past 1400 yr, associated with changing modes of atmospheric circulation over Eurasia based on glaciochemical series from the GISP2 Ice Core (Mayewski et al., 1994; O'Brien et al., 1995). Here, we examine the general state of the atmosphere in western Central Asia during the past 1500 yr, based on changing deposition of Ti representing aeolian detrital inputs in Core

https://doi.org/10.1016/j.yqres.2006.12.003 Published online by Cambridge University Press

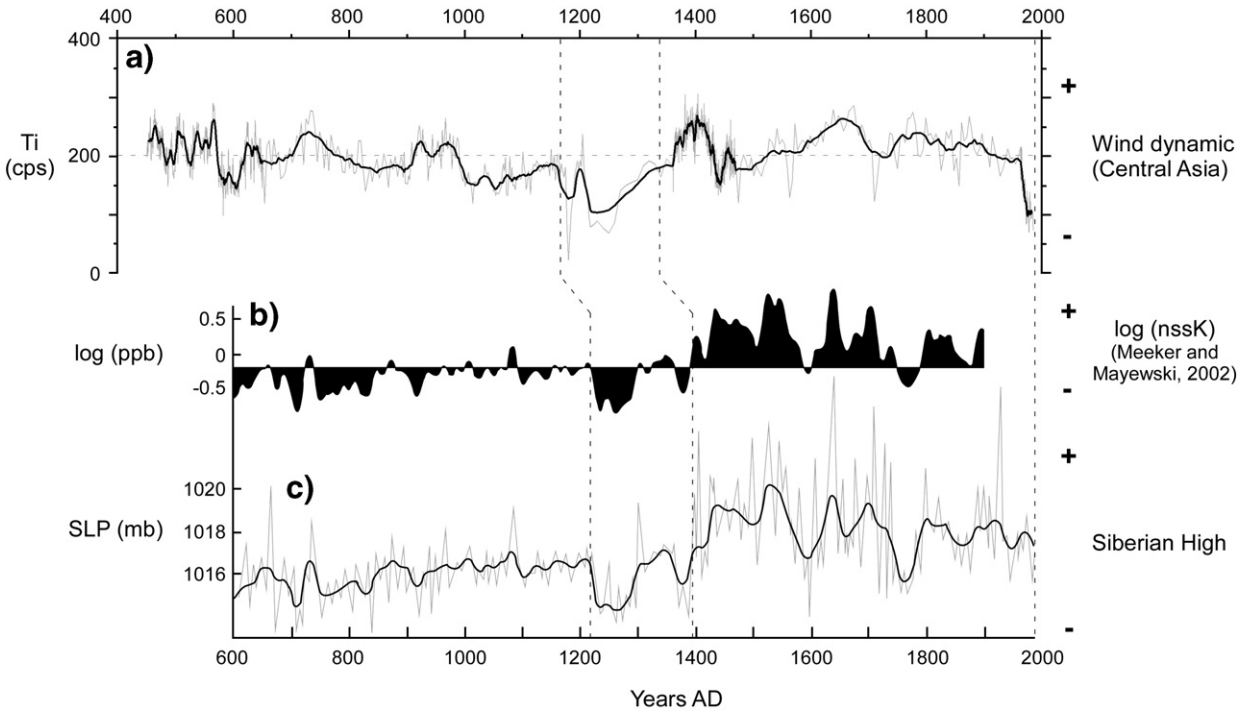

Figure 7. Comparison between (a) the titanium record of Core CH1 from the Large Aral Sea, (b) the non-seasalt Potassium (nssK) and (c) the Siberian High records of Meeker and Mayewski (2002). Bold curves (a, c) represent smoothed data using an 11-yr and 20-yr running average for titanium and nssK-Siberian High records, respectively.

CH1, and compare it with the SH record of Meeker and Mayewski (2002) (Fig. 7). Our site location, in the continental interior of Asia where the dust storms are generated, may even represent a more sensitive area for characterizing changes in circulation pattern in western Central Asia.

Based on low content of Ti and nssK in Cores CH1 and GISP2 (Fig. 7), respectively, relatively weak spring (i.e., March–April–May or MAM) SH characterize the period AD 700–1150, with the prevalence of a more zonal circulation. Prior to AD 700 (AD 600–700), the intensity of the SH fluctuate at high values, underlying a stronger atmospheric circulation. This period follows a phase of stronger and more westward extending SH from AD 450–600, as reflected by increased deposition of Ti in the Aral Sea.

The Medieval Warm Period (MWP; ca. AD 1000–1400) and Little Ice Age (LIA; ca. AD 1400–1800) provide the most suitable recent analogues for naturally warmer and colder than present climate (Crowley, 2000; Bradley, 2003). During the late MWP (AD 1200–1400), aeolian detrital markers in Core CH1 exhibit two abrupt shifts assignable to a pronounced modification of atmospheric circulation in western Central Asia during early spring. Significant weaker (and more eastward) SH are inferred between ca. AD 1180–1210 and ca. AD 1265–1310 from minimal deposition of Ti (see also Fig. 6), suggesting the onset of prevailing zonal circulation, whereas intermediate periods (ca. AD 1210–1265; ca. AD 1310–1400) are indicative of moderately stronger SH with a more meridional MAM circulation. Similar features are observed in nssK concentrations from Greenland (Meeker and Mayewski, 2002), although the timing of these events slightly differs (Fig. 7). A possible explanation for these discrepancies can be the errors assigned to dating for both age models. In the GISP2 Ice Core, the current estimated age error is 2% for the time span 0–11,640 cal yr BP, which corresponds to about 40 yr (Alley et al., 1993; Meese et al., 1994). In our age model, age uncertainty as discussed in the Chronology section indicates a possible error of ca. 65 yr between AD 1200 and AD 1400.

At the transition from MWP to LIA, the dominant mode of atmospheric circulation changed, coinciding with a transition from a period of relatively weak MAM SH to one in which the MAM circulation greatly intensified throughout the LIA (Meeker and Mayewski, 2002). This change in pressure distribution in Asia explains the increasing concentration of nssK in the GISP2 Ice Core between AD 1400 and about AD 1750. We would thus expect to show an imprint of this atmospheric change on the wind dynamics in western Central Asia. Comparing the dust flow pattern from Core CH1 (Ti) with concentrations of nssK (Fig. 7), we observe that in the Aral Sea the dust input was increasing at ca. AD 1350 and remained high until about AD 1750, indicating the prevalence of a more meridional atmospheric circulation in Central Asia. Subsequently, a prominent coeval decrease in Ti and nssK contents documents weaker MAM SH between AD 1750 and AD 1800.

In contrast, the period AD 1800–1980 records intensified (and more westward) MAM SH in western Central Asia, as reflected by elevated input of aeolian particles in the Aral Sea and relatively high concentrations of nssK in Greenland. In most recent sediments, a significant decrease in the frequency of dust storms occurs after AD 1980. This phenomenon has been recorded in other studies (Usmanov, 1968; Chub, 1998; Galaeva,

https://doi.org/10.1016/j.yqres.2006.12.003 Published online by Cambridge University Press

1998; Meeker and Mayewski, 2002), associated with prominent change in the atmospheric circulation pattern towards a weakening of the SH and a more zonal flow over East Asia (Savelieva et al., 1991; Clark et al., 1999; Panagiotopoulos et al., 2005). The decrease in the intensity of the SH may be linked with the global warming of the atmosphere, and it is expected to amplify by the forthcoming years (Druyan and Rind, 1991).

Conclusions

Based on very high-resolution microfacies and inorganic geochemical analyses, we report important changes in wind strength and frequency in the Aral Sea basin during the past 1500 yr. Changes in wind dynamics in western Central Asia, as based on Ti content in Core CH1, correlate prominently with the non-sea salt potassium (nssK) record of the GISP2 Ice Core (Meeker and Mayewski, 2002). Therefore, these changes appear to be controlled by the intensity of the Siberian High (SH) pressure system during early spring which modulates the atmospheric circulation system over western Central Asia.

During AD 450–700, ca. AD 1210–1265, ca. AD 1350–1750 and AD 1800–1975, more pronounced meridional atmospheric circulation associated with stronger and more westward extending SH prevailed in the Aral Sea basin, leading to the intensification of anticyclonic conditions over the region during early spring. It contrasts with other time intervals where the influence of the SH was noticeably weakened. During ca. AD 1180–1210 and AD 1265–1310, lower sedimentation rates associated with decreasing detrital inputs and lamination thickness characterize substantial reduced dust storm frequency in the Aral Sea basin, consistent with decreasing concentration of nssK transported from Asia in the GISP2 Ice Core. Therefore, these periods bear witness to a waning of anticyclonic conditions in western Central Asia associated to a more zonal atmospheric circulation.

Other climate forcing may play a significant role in the regulation of seasonal temperature and pressure gradients that determine the intensity and the frequency of dust storms in Central Asia. By now the impact of the Tibetan thermal forcing, which today plays an important role on ocean–atmosphere–land interactions during the summer season, has not been studied yet in sedimentary archives. Future investigations may show whether the Aral Sea sediments also hold information on past changes of the Tibetan thermal forcing, and to which extent it does influence the hot desert climate of Central Asia.

Acknowledgments

The CLIMAN project was funded by INTAS (European Union) (Project No Aral 00-1030) and the German Science Foundation (DFG Project 436 RUS 111/663-OB 86/4). We are indebted to them for this support. We are grateful to Prof. Dr. Tomasz Goslar (Poznañ Radiocarbon Laboratory, Poland) for providing high-quality AMS ^{14}C dating. We also thank Hans von Suchodoletz for his help during XRD measurements. The authors gratefully acknowledge Dr. Derek B. Booth and two anonymous reviewers for their constructive comments which have helped to improve the manuscript.

References

Aizen, E.M., Aizen, V.B., Melack, J.M., Nakamura, T., Ohta, T., 2001. Precipitation and atmospheric circulation patterns at mid-latitudes of Asia. International Journal of Climatology 21, 535–556.

Alley, R.B., Meese, D.A., Shuman, C.A., Gow, A.J., Taylor, K.C., Grootes, P.M., White, J.W.C., Ram, M., Waddington, E.D., Mayewski, P.A., Zielinski, G.A., 1993. Abrupt increase in Greenland snow accumulation at the end of the Younger Dryas event. Nature 362, 527–529.

Austin, P., Mackay, A., Palagushkina, O., Leng, M., 2007. A high-resolution diatom-inferred palaeoconductivity and lake level record of the Aral Sea for the last 1600 yr. Quaternary Research 67, 383–393.

Barlow, M.H., Cullen, B., 2002. Drought in Central and southwest Asia: La Niña, the warm pool and the Indian precipitation. Journal of Climate 15 (7), 697–700.

Bolle, M.P., Adatte, T., 2001. Palaeocene-early Eocene climatic evolution in the Tethyan realm: clay mineral evidence. Clay Minerals 36 (2), 249–261.

Bond, G., Kromer, B., Beer, J., Muscheler, R., Evans, M.N., Showers, W., Hoffmann, S., Lotti-Bond, R., Hajdas, I., Bonani, G., 2001. Persistent solar influence on North Atlantic climate during the Holocene. Science 294, 2130–2136.

Bradley, R.S., 2000. 1000 years of climate change. Science 288, 1353–1354.

Bradley, R.S., 2003. Climate of the last Millenium. Holocene Working Group Workshop, Bjerknes Centre for Climate Research, August 2003.

Briffa, K.R., 2000. Annual climate variability in the Holocene: interpreting the message of ancient trees. Quaternary Science Reviews 19, 87–105.

Chub, V.E., 1998. Estimation of aerosol influence on climatic characteristics of the Aral Sea basin (Otzenka vliyaniya aerozolei na klimaticheskie kharakteristiki baseina Aral'skogo moray). Problems of Desert Development 3–4, 50–55 (in Russian).

Clark, M.P., Serreze, M.C., Robinson, D.A., 1999. Atmospheric controls on Eurasian snow extent. International Journal of Climatology 19, 27–40.

Cook, E.R., Esper, J., D'Arrigo, R.D., 2004. Extra-tropical Northern Hemisphere land temperature variability over the past 1000 years. Quaternary Science Reviews 23, 2063–2074.

Crowley, T.J., 2000. Causes of climate change over the past 1000 years. Science 289, 270–277.

Demory, F., Oberhänsli, H., Nowaczyk, N.R., Gottschalk, M., Wirth, R., Naumann, R., 2005. Detrital input and early diagenesis in sediments from Lake Baikal revealed by rock magnetism. Global and Planetary Change 46, 145–166.

Druyan, L.M., Rind, D., 1991. Implications of climate change on a regional scale. In: Graber, M., Cohen, A., Magaritz, M. (Eds.), Proceedings of the International Workshop on Regional Implications of Future Climate Change, September 1993, vol. 311, pp. 75–78.

Duan, A.M., Wu, G.X., 2005. Role of the Tibetan Plateau thermal forcing in the summer climate patterns over subtropical Asia. Climate Dynamics 24, 793–807.

Friedrich, J., Oberhänsli, H., 2004. Hydrochemical properties of the Aral Sea water in summer 2002. Journal of Marine Systems 47, 77–88.

Galaeva, O.S., 1998. On the monitoring of carrying out of sandy salty aerosol from drained part of bottom of the Aral Sea (K monitoringu vinosa peschanih I solevih aerosolei s visohshego dna Aral'skogo moray). Problems of Desert Development 3–4, 17–21 (in Russian).

Gruza, G.V., Ran'kova, E.Ya., Kleschenko, L.K., Aristova, L.N., 1999. Relationship between climatic anomalies on territory of Russia and phenomena El Nino-South Oscillation. Meteorology and Hydrology 5, 32–51 (in Russian).

Heim, C., 2005. Die Geochemische Zusammensetzung der Sedimente im Aralsee und Sedimentationsprozesse während der letzten 100 Jahre. Diploma thesis, Alfred-Wegener-Institut für Polar-und Meeresforschung, Bremerhaven. 89 pp.

Jansen, J.H.F., van der Gaast, S.J., Koster, B., Vaars, A., 1998. CORTEX, a shipboard XRF-scanner for element analyses in split sediment cores. Marine Geology 151, 143–153.

Khan, V.M., Vilfand, R.M., Zavialov, P., 2004. Long-term variability of air temperature in the Aral sea region. Journal of Marine Systems 47, 25–33.

Létolle, R., Mainguet, M., 1993. Aral. Springer Verlag, Paris. 358 pp.

Lioubimtseva, E., 2002. Arid environments. In: Shahgedanova, M. (Ed.), Physical Geography of Northern Eurasia. Oxford University Press, Oxford. 571 pp.

Lioubimtseva, E., Cole, R., Adams, J.M., Kapustin, G., 2005. Impacts of climate and land-cover changes in arid lands of Central Asia. Journal of Arid Environments 62, 285–308.

Mainguet, M., Létolle, R., Dumay, F., 2002. Le système régional d'action éolienne (SRAE) du bassin de l'Aral (Kazakhstan, Ouzbékistan et Turkménistan). C.R. Geosciences 334, 475–480.

Mann, M.E., Jones, P.D., 2003. Global surface temperatures over the past two millennia. Geophysical Research Letters 30 (15), 1820, doi:10.1029/2003GL017814, 2003.

Mayewski, P.A., Meeker, L.D., Whitlow, S., Twickler, M.S., Morrison, M.C., Bloomfield, P., Bond, G.C., Alley, R.B., Gow, A.J., Grootes, P.M., Meese, D.A., Ram, M., Taylor, K.C., Wumkes, W., 1994. Changes in atmospheric circulation and ocean ice cover over the North Atlantic during the last 41,000 years. Science 261, 195–197.

Meeker, L.D., Mayewski, P.A., 2002. A 1400-year high-resolution record of atmospheric circulation over the North Atlantic and Asia. The Holocene 12 (3), 257–266.

Meese, P.M., Alley, R.B., Gow, A.J., Grootes, P., Mayewski, P.A., Ram, D.A., Taylor, K.C., Waddington, E.D., Zielinski, G., 1994. Preliminary Depth-Age Scale of the GISP2 Ice Core. U.S. Army Cold Regions Research Laboratory Publication SR94-01, Hanover, NH.

Middleton, N.J., 1986. Geography of dust storms in South-West Asia. Journal of Climatology 6, 183–196.

Moberg, A., Sonechkin, D.M., Holmgren, K., Datsenko, N.M., Karlén, W., 2005. Highly variable northern temperatures reconstructed from low- and high-resolution proxy data. Nature 433, 613–617.

Nezlin, N.P., Kostianoy, A.G., Li, B.-L., 2005. Inter-annual variability and interaction of remote-sensed vegetation index and atmospheric precipitation in the Aral Sea region. Journal of Arid Environments 62, 677–700.

Nourgaliev, D.K., Heller, F., Borisov, A.S., Hajdas, I., Bonani, G., Iassonov, P. G., Oberhänsli, H., 2003. Very high resolution paleosecular variation record for the last 1200 years from the Aral Sea. Geophysical Research Letters 30 (17), 4-1–4-4.

O'Brien, S.R., Mayewski, P.A., Meeker, L.D., Meese, D.A., Twickler, M.S., Whitlow, S.I., 1995. Complexity of Holocene climate as reconstructed from a Greenland ice core. Science 270, 1962–1964.

Orlovsky, L., Orlovsky, N., 2002. White sand storms in Central Asia. In: Yang, Youlin, Squires, V., Lu, Qi (Eds.), Global Alarm: Dust and Sand Storms from the World's Drylands. UNCCD, Bangkok, pp. 169–201.

Orlovsky, L., Orlovsky, N., Durdyev, A., 2005. Dust storms in Turkmenistan. Journal of Arid Environments 60, 83–97.

Panagiotopoulos, F., Shahgedanova, M., Hannachi, A., Stephenson, D.B., 2005. Observed trends and teleconnections of the Siberian High: a recently declining center of action. Journal of Climate 18, 1411–1422.

Petschick, R., 2000. MacDiff 4.2.5 Bedienungsanleitung (http://servemac.geologie.uni-frankfurt.de/Rainer/html).

Reimer, P.J., Baillie, M.G.L., Bard, E., Bayliss, A., Beck, J.W., Bertrand, C.J.H., Blackwell, P.G., Buck, C.E., Burr, G.S., Cutler, K.B., Damon, P.E., Lawrence Edwards, R., Fairbanks, R.G., Friedrich, M., Guilderson, T.P., Hogg, A.G., Hughen, K.A., Kromer, B., McCormac, G., Manning, S., Bronk Ramsey, C., Reimer, R.W., Remmele, S., Southon, J.R., Stuiver, M., Talamo, S., Taylor, F.W., van der Plicht, J., Weiyhenmeyer, C.E., 2004. IntCal04 terrestrial radiocarbon age calibration, 0–26 cal. yr BP. Radiocarbon 46 (3), 1029–1058.

Roberts, N., Wright, H.E., 1993. Vegetational, lake-level, and climatic history of the Near East and Southwest Asia. In: Wright, H.E. (Ed.), Global Climates since the Last Glacial Maximum. University of Minnesota Press, pp. 194–220.

Röhl, U., Abrams, L.J., 2000. High-resolution, downhole and non-destructive core measurements from Sites 999 and 1001 in the Carribean Sea: application to the Late Paleocene Thermal Maximum. Proceedings of the Ocean Drilling Program (ODP) Scientific Results, vol. 165. Ocean Drilling Programm, College Station, TX, pp. 191–204.

Rohling, E.J., Mayewski, P.A., Abu-Zied, R.H., Casford, J.S.L., Hayes, A., 2002. Holocene atmosphere–ocean interactions: records from Greenland and the Aegean Sea. Climate Dynamics 18, 578–593.

Romanov, N.N., 1961. Dust storms in Central Asia (Pyl'nye buri Srednei Asii). Samarkand University, Tashkent. 198 pp. (in Russian).

Romanov, N.N., 1986. Forecast of dust storms and advective dust haze. Instruction in short-term weather forecasts, Central Asia. Gidrometeoizdat Leningrad 2 (3), 210–216 (in Russian).

Sahsamanoglou, H.S., Makrogiannis, T.J., Kallimopoulos, P.P., 1991. Some aspects of the basic characteristics of the Siberian anticyclone. International Journal of Climatology 11, 827–839.

Savelieva, N.I., Semiletov, I.P., Vasilevskaya, L.N., Pugach, S.P., 1991. A climate shift in seasonal values of meteorological and hydrological parameters for Northeastern Asia. Progress in Oceanography 47, 279–297.

Seredkina, E.A., 1960. Dust storms in Kazakhstan (Pyl'nie buri v Kazakhstane). Proceedings of KazNIGMI 15, 54–59 (in Russian).

Singer, A., Zobeck, T., Poberezsky, L., Argaman, E., 2003. The PM_{10} and $PM_{2.5}$ dust generation potential of soils/sediments in the Southern Aral Sea Basin, Uzbekistan. Journal of Arid Environments 54, 705–728, doi:10.1006/jare.2002.1084.

Small, E.E., Giorgi, F.G., Sloan, L.S., Hostetler, S., 2001. The effects of desiccation and climatic change on the hydrology of the Aral Sea. Journal of Climate 14, 300–322.

Sorrel, P., 2006. The Aral Sea: a palaeoclimate archive. PhD thesis, University Potsdam (Germany) and University Claude Bernard-Lyon I (France). 109 pp.

Sorrel, P., Popescu, S.-M., Head, M.J., Suc, J.P., Klotz, S., Oberhänsli, H., 2006. Hydrographic development of the Aral Sea during the last 2000 years based on a quantitative analysis of dinoflagellate cysts. Palaeogeography, Palaeoclimatology, Palaeoecology 234 (2–4), 304–327.

Sorrel, P., Popescu, S.-M., Klotz, S., Suc, J.P., Oberhänsli, H., 2007. Climate variability in the Aral Sea basin (Central Asia) during the late Holocene based on vegetation changes. Quaternary Research 67 (3), 357–370.

Subbotina, O.I., 1995. Atmospheric circulation. In: Muminova, F.A., Inagamova, S.I. (Eds.), Change of Climate in Middle Asia. SARNIIGMI Publishing, Tashkent, pp. 8–34 (in Russian).

Usmanov, V.O., 1968. Estimation of the influence of dusty salt transfer on the productivity of agricultural crops in the Priaral region (Otzenka vliyaniya sole-pyleperenosa na productivnost' sel'skohozyaistvennih kultur v Priaral'skom regione). Problems of Desert Development 3–4, 147–151 (in Russian).

Zavialov, P.O., 2005. Physical Oceanography of the Dying Aral Sea. Springer Verlag, published in association with Praxis Publishing, Chichester, UK. 146 pp.

Zolotokrylin, A.N., 1996. Dust storms in Turanian Lowland. Proceedings of Russian Academy of Sciences Geographic Series 6, 48–54 (in Russian).